Supporting Information

Double charge transfer mechanistic insights into the tailoring of BiOI nanoplates and boron-doped graphitic carbon nitride: A 2D/2D anchored p-n heterojunction nanocatalyst for improved photodegradation

Pragnyashree Aparajita, Shubhalaxmi Choudhury, Ugrabadi Sahoo, Samarjit Pattnayak, Sandip Padhiari, Manamohan Tripathy and Garudadhwaj Hota*

Department of Chemistry, NIT Rourkela, Odisha, India, 769008.

*Corresponding Author

Dr. Garudadhwaj Hota

Department of Chemistry, NIT Rourkela, Rourkela, Odisha, India, 769008

Email: garud@nitrkl.ac.in, garud31@yahoo.com

Ph: 91-661-2462655

Fax: 91-661-246265

Contents in the Supporting Information

Characterization Techniques

Fig. S1. Digital images of the synthesized (a) $g-C_3N_4$, (b) BCN, (c) BiOI, and (d) BiOI/BCN-15 nanocomposite.

Fig. S2. (a, b) FESEM Elemental Mapping of BiOI/BCN-15; (c-h) FESEM Energy Dispersive X-Ray Spectroscopy of BiOI/BCN-15 nanocomposite photocatalyst (i) EDX Analysis of BiOI/BCN-15 nanocomposite.

Fig. S3. XPS Survey Spectra of BiOI/BCN-15

TableS1. Comparison Table depicting the difference in Surface Area, Pore Volume, and Pore Diameters of the Synthesized Nanocomposite

Fig. S4. (a)UV-DRS plot of BCN, BiOI, BiOI/BCN-5, BiOI/BCN-10, BiOI/BCN-15, BiOI/BCN-20 (Inset Plot represents the difference in absorbance of the as-prepared photocatalysts); (b) Tauc plot of the nanocomposite photocatalyst BiOI/BCN-15

Fig. S5. PL spectra of the precursors and the fabricated nanocomposites

Table S2. (a)Work overview in recent years showing the use of BiOI and BCN for the degradation of numerous antibiotics.

(b) Work overview in recent years showing the use of BiOI and BCN for the degradation of numerous dyes.

Fig. S6. Degradation plots for (a) Neutral red, (b) Methyl orange, (c) Methylene blue of the precursors and the fabricated nanocomposites under visible light irradiation; First order rate kinetics plots for (a) Neutral red, (b) Methyl orange, (c) Methylene blue; Comparison plot for first order rate constants of BCN, BiOI and fabricated nanocomposites for (a) Neutral red, (b) Methyl orange, (c) Methylene blue respectively.

Fig. S7. HRMS spectra of TCH after degradation

Table S3. The degradation products obtained through HRMS Analysis

Fig. S8. (a) LCMS spectra of TCH after degradation; (b) Degradation pathway demonstrating the intermediate products

Fig. S9. Percentage removal of total organic carbon at different time intervals

Fig. S10. ESR spectra representing a generation of (a) ·OH radicals, (b) ·O_2^- radicals in light and dark conditions respectively.

Fig. S11. Reusability Survey of the fabricated nanocatalyst for degradation of the target pollutant.

Fig. S12. XRD of the fabricated nanocatalyst before and after four consecutive cycles.

Fig. S13. FESEM of Nanocomposite BiOI/BCN-15 before and after photocatalytic degradation.

Characterization techniques:

A multipurpose X-ray diffraction (XRD) machine (Rigaku, Ultima-IV) was used to inspect the purity of phase and crystalline analysis of the manufactured BiOI/BCN-x nanocomposites using Ni-filtered Cu Kα (λ=1.5418 A°) radiation. For investigating the chemical alteration or modification in the structure, a Fourier transform Infrared Spectroscopic (FT-IR) study on KBr pellets was conducted using a PerkinElmer Infrared spectrophotometer. Furthermore, to measure the UV spectra of the corresponding nanocomposites, a Jasco V-650 spectrometer in diffused reflectance mode was used. Herein, $BaSO_4$ was chosen as the reference in the wavelength range of 200-800 nm. The surface morphology of the composites was studied using FESEM technique (M, Nova NanoSEM FEI microscope)) and the microstructural analysis was done using HRTEM (Tecnai 300 kV). The compositional analysis of the nanocomposites was done using energy-dispersive X-Ray spectroscopy (EDS) [through Bruker EDSQUANTAX] and X-Ray photoelectron spectroscopy (XPS) [PHI 5000 versa probe III equipment]. Also, the HORIBA Scientific spectrofluorimeter (Fluromax-4) was used for photoluminescence analysis at an excitation wavelength of 365 nm to analyze the recombination rate. An electrochemical analyzer (PSM 1735) fortified with a three-electrode system was subsequently used for electrochemical analysis. In this case, Platinum wire was used as the counter electrode, and Ag/AgCl electrode was ascribed as the reference electrode in 0.1 M Na_2SO_4 electrolyte. Fluorine-doped tin oxide (FTO) coated with the required photocatalyst served as the working electrode for the Mott-Schottky analysis at a frequency of 1000 MHz. At zero biased potential, the impedance analysis was captured. For the detection of ·OH radicals, 0.01 g of the photocatalyst was mixed with 50 μL DMPO in 0.5 mL of deionised water and the solution was agitated thoroughly. Thereafter, using 100 μL capillary tube, the sample was inserted into ESR cavity and tested. Similarly, for the detection of $·O_2^-$ radicals, the above process was repeated using 0.5 mL of methanol instead of deionized water. The Malvern Zetasizer device (Malvern Nano ZS, USA) was also used to measure the Zeta potential. To determine the pH of the solution, a digital pH meter from Sartorius Mechatronics India Pvt. Ltd. equipped with a glass electrode was employed. Additionally, utilizing Quantachrome, Autoabsorb-IQ physisorption equipment, the surface area, and porosity data were calculated from nitrogen adsorption-desorption analysis.
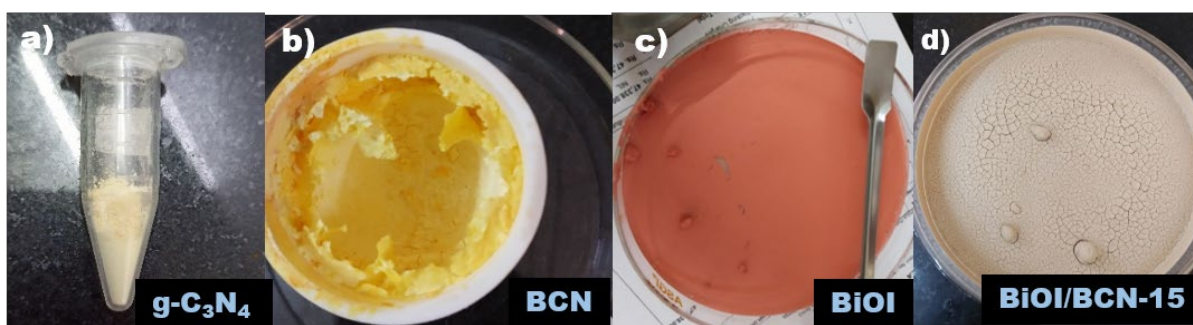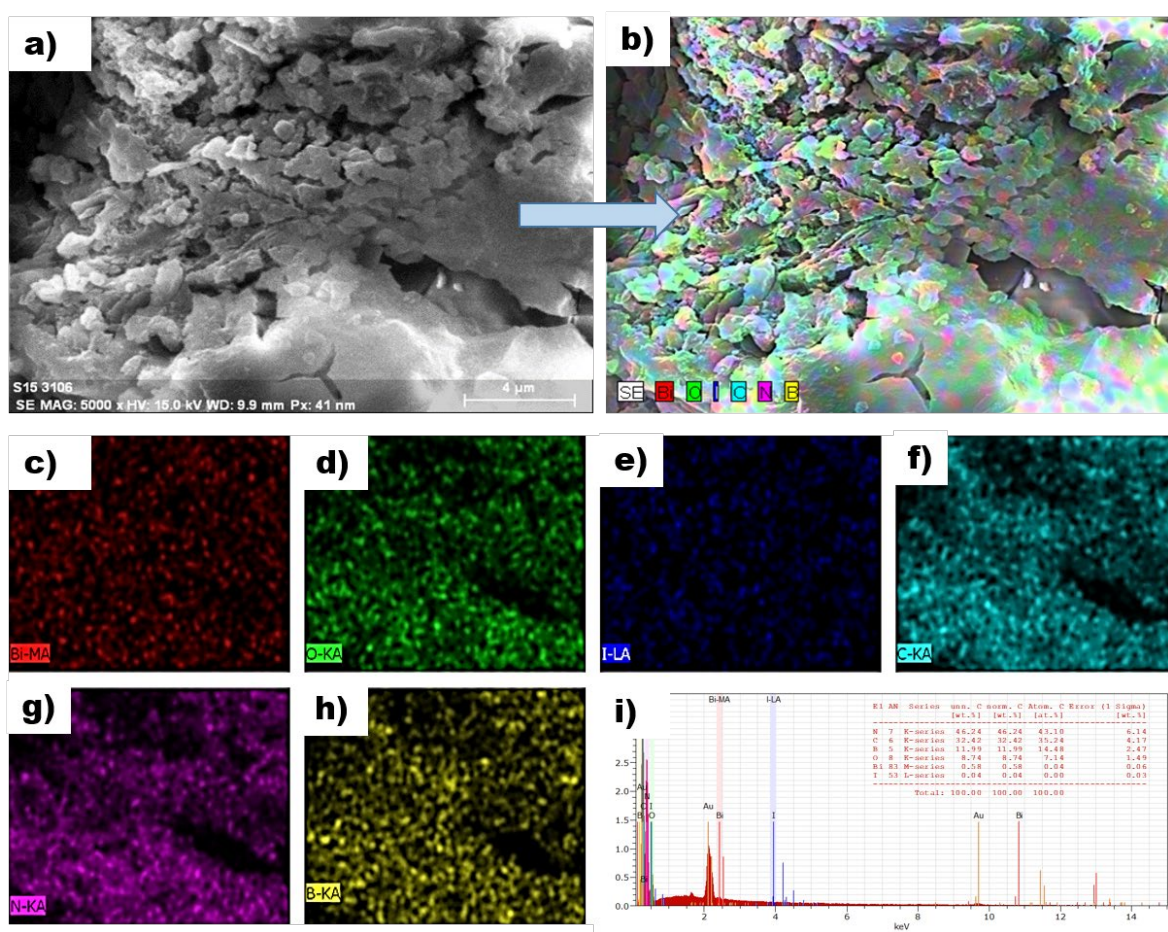
Fig. S1. Digital images of the synthesized (a) g-C$_3$N$_4$, (b) BCN, (c) BiOI, and (d) BiOI/BCN-15 nanocomposite.

S2.

Fig. S2. (a, b) FESEM Images of BiOI/BCN-15; (c-h) FESEM Elemental Mapping of BiOI/BCN-15 heterostructure; (i) FESEM Energy Dispersive X-Ray Spectroscopy of BiOI/BCN-15 nanocomposite photocatalyst.
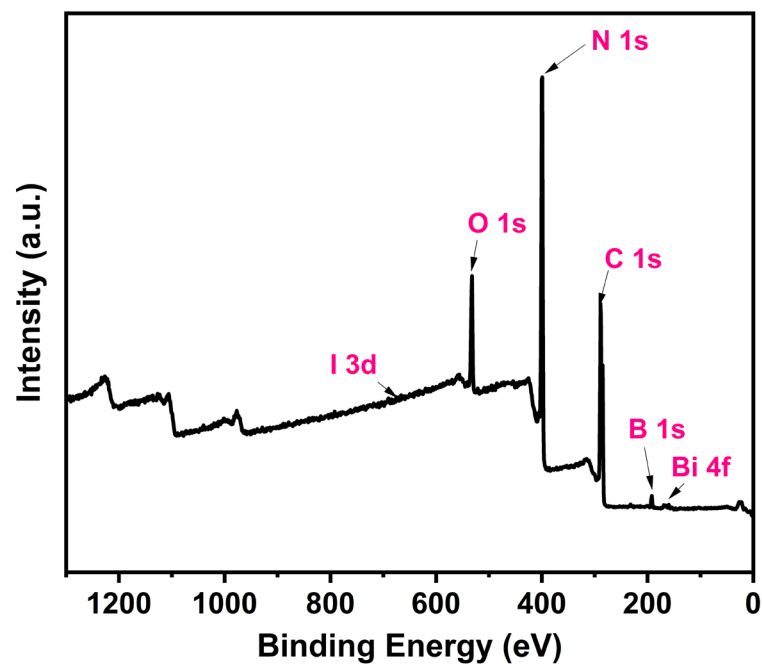
Fig. S3. XPS Survey Spectra of BiOI/BCN-15

Table S1. Comparison Table depicting the difference in Surface Area, Pore Volume, and Pore Diameters of the Synthesized Nanocomposite.

S.L No.	SAMPLE NAME	SURFACE AREA (m^2 g^{-1})	PORE VOLUME (cc/g)	PORE DIAMETER (m^2/g)
1	BIOI/BCN-5	2.565	0.010	3.939
2	BIOI/BCN-10	5.299	0.035	3.909
3	BIOI/BCN-15	44.987	0.063	3.927
4	BIOI/BCN-20	2.668	0.004	3.503
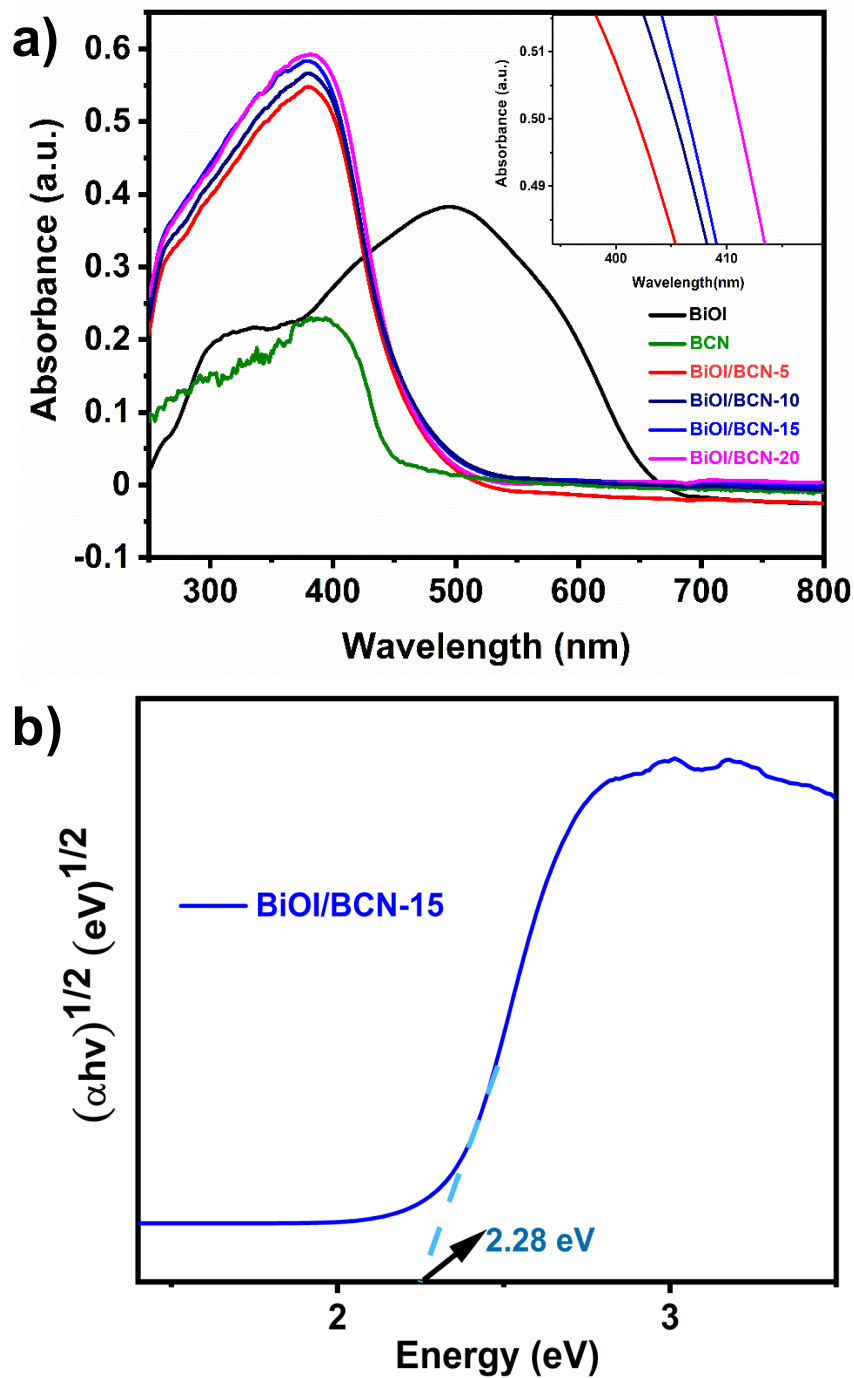
Fig. S4. (a) UV-DRS plot of BCN, BiOI, BiOI/BCN-5, BiOI/BCN-10, BiOI/BCN-15, BiOI/BCN-20(Inset Plot represents the difference in absorbance of the as-prepared photocatalysts); (b) Tauc plot of the nanocomposite photocatalyst BiOI/BCN-15.
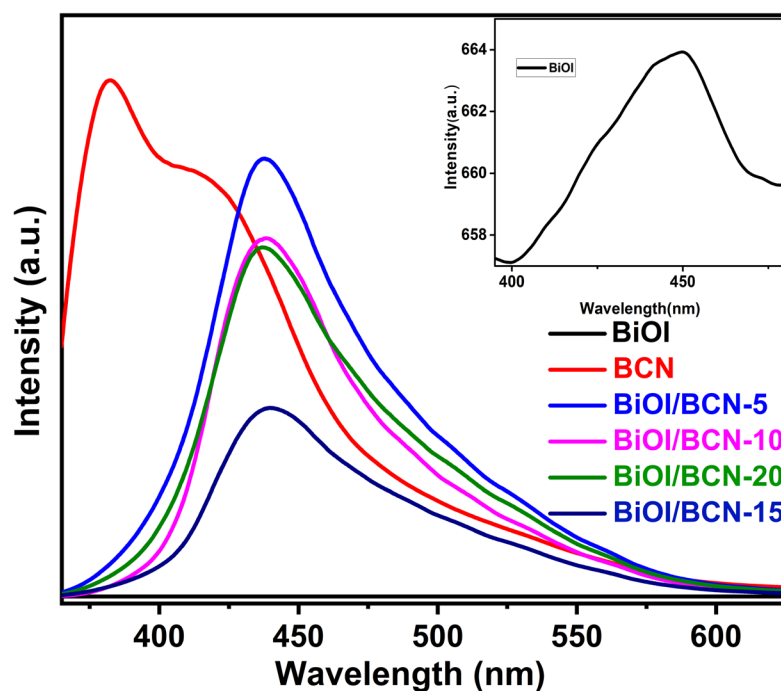
Fig. S5. PL spectra of the precursors and the fabricated nanocomposites.

Table S2. (a)Work overview in recent years showing the use of BiOI and BCN for the degradation of numerous antibiotics.; (b) Work overview in recent years showing the use of BiOI and BCN for the degradation of numerous dyes.

(a)

Photocatalyst	Initial TCH conc., degradation %	Catalyst activity time (min)	Source of Light used for Degradation	Catalyst dosage (mg)	TCH (mL)	References
ZnTCPP/g-C$_3$N$_4$	30 ppm, 80.3 %	120	Visible light	150 mg	50	1
Bi$_4$O$_5$Br$_2$/ MWCNT	20 ppm, 86.2 %	120	Visible light	20 mg	100	2
BiPO4/GA	20 ppm ,81.65%	80	UV-Visible light	25 mg	50	3
BiOI/BCN	*40 ppm, 87.45 %*	*60*	*Visible light*	*40 mg*	*500*	*Current paper*

(b)

Photocatalyst	Initial RhB conc., degradation %	Catalyst activity time (min)	Source of Light used for Degradation	Catalyst dosage (mg)	RhB (mL)	References
$Bi_4O_5Br_2$/ MWCNT	20 ppm,83.1%	75	Visible light	30 mg	100	2
g-C_3N_4/Fe_3O_4/ AgCl	10 ppm, 49.5%	180	Visible light	100 mg	250	4
Silicate Ceramics	10 ppm, <88 %	120	UV radiation	50 mg	200	5
BiOI/BCN	*10 ppm, 85.33 %*	*60*	*Visible light*	*40 mg*	*250*	*Current paper*
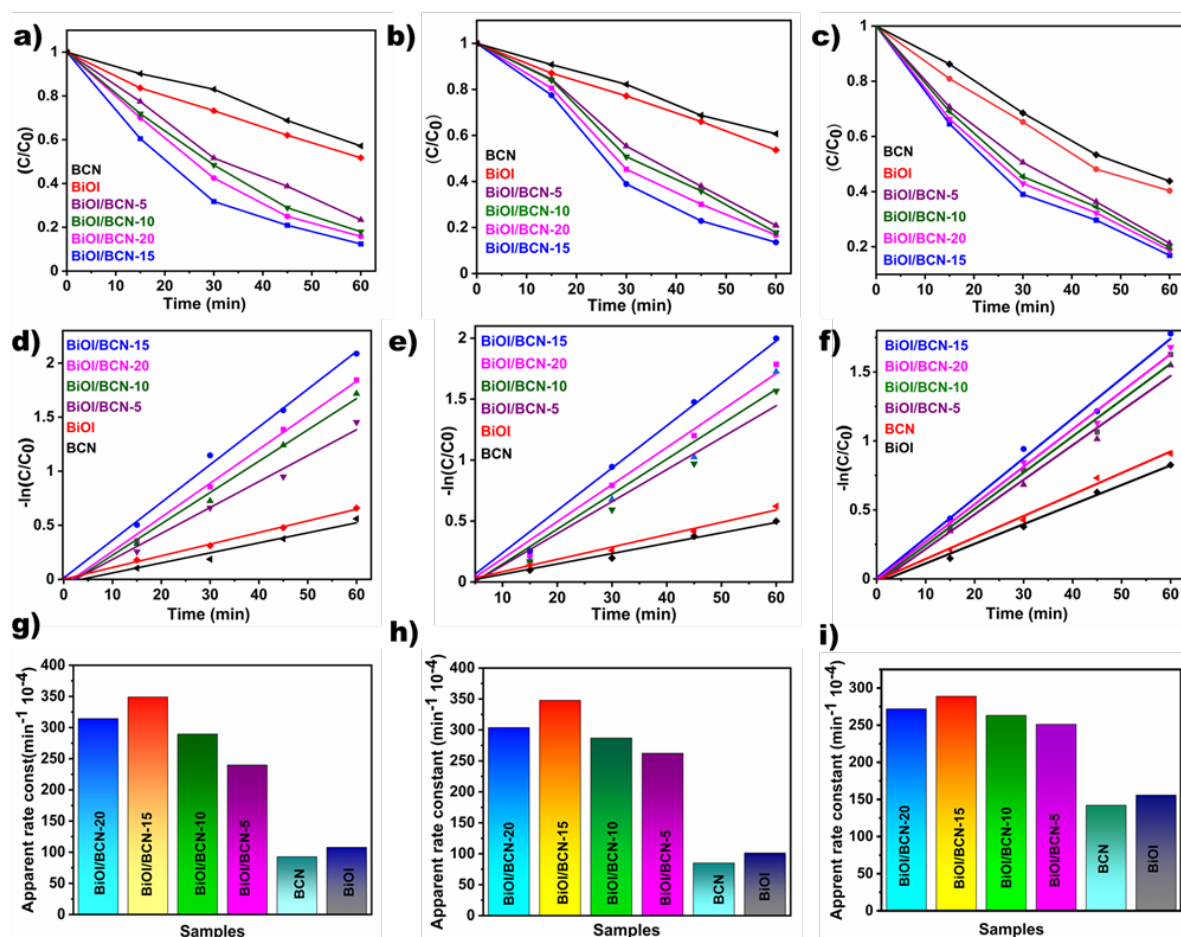
Fig. S6. (a-c) Degradation plots for Neutral red, Methyl orange, and Methylene blue of the precursors and the fabricated nanocomposites under visible light irradiation;(d-f) First order rate kinetics plots for Neutral red, Methyl orange, and Methylene blue; (g-i) Comparison plot for first

order rate constants of BCN, BiOI and fabricated nanocomposites for Neutral red, Methyl orange, and Methylene blue respectively.
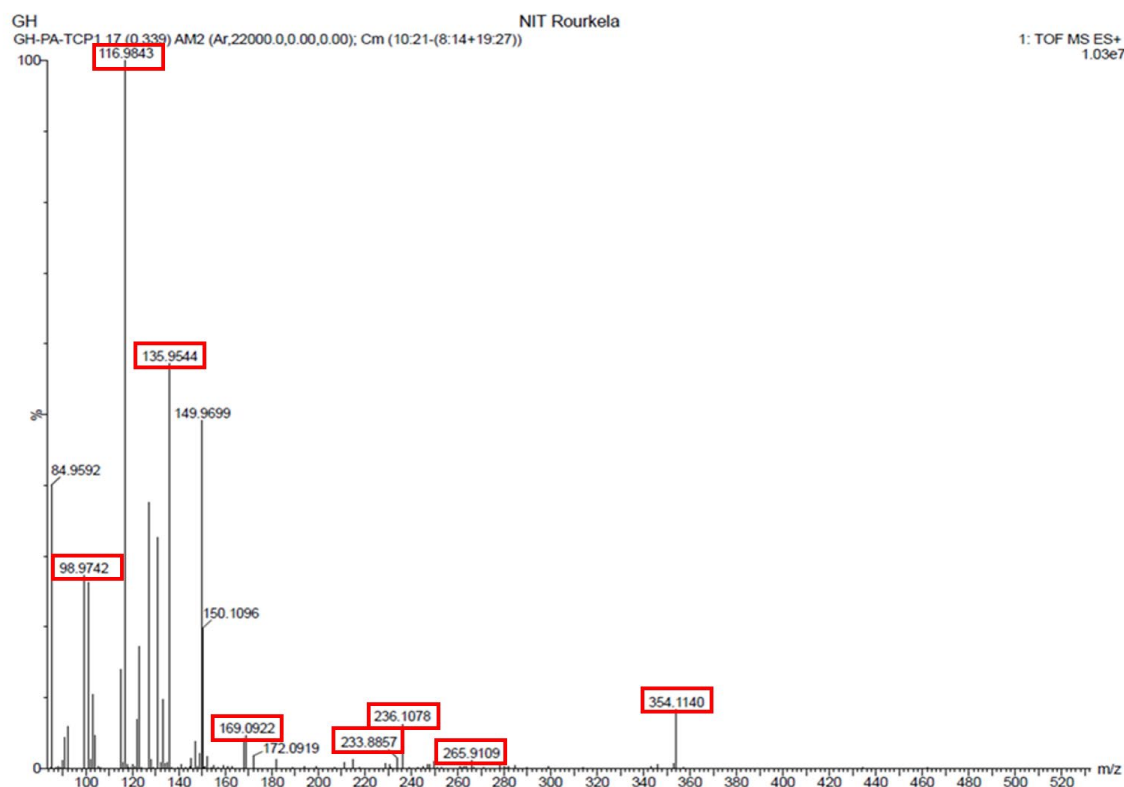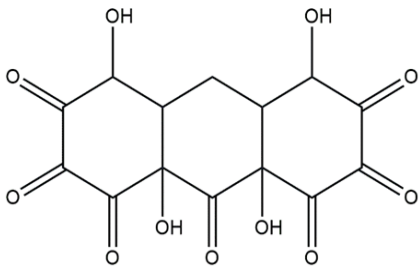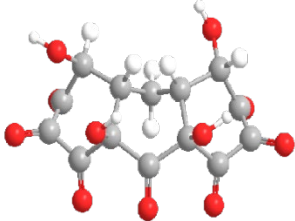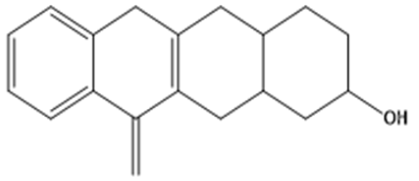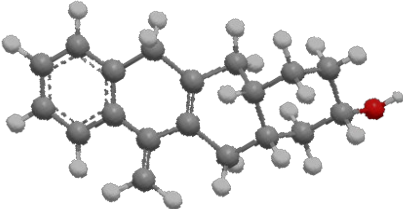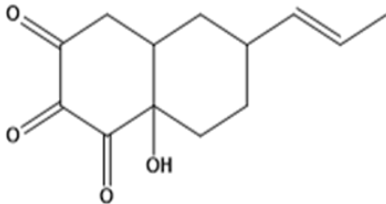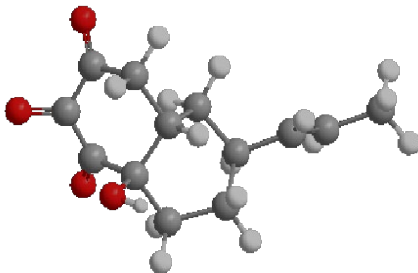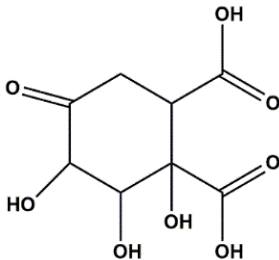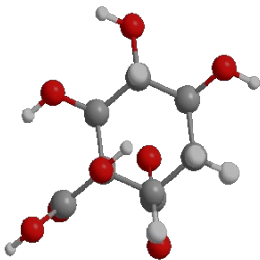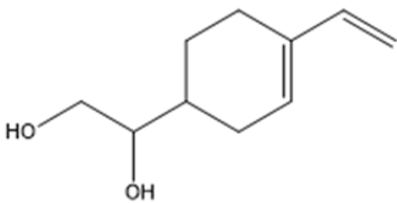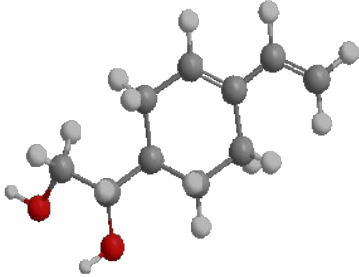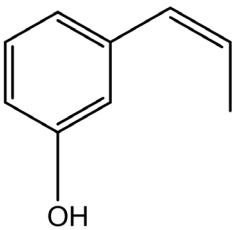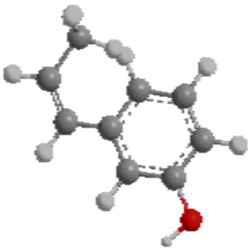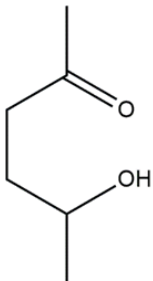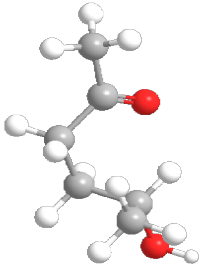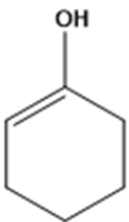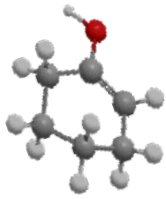

Fig. S7. HRMS spectra of TCH after degradation

Table S3. The possible degradation products obtained through HRMS Analysis.

Sl. No.	Found m/z value through HRMS	Calculated value	Pseudo molecular structure	Plausible Structure	3D structural representation
1	354.1140	354.0223	[M]$^+$		
2	265.9109	266.1671	[M-H]$^+$		
3	236.1078	236.1049	[M]$^+$		
4	233.8857	234.0376	[M-H]$^+$		
5	169.0922	168.1150	[M+H]$^+$		

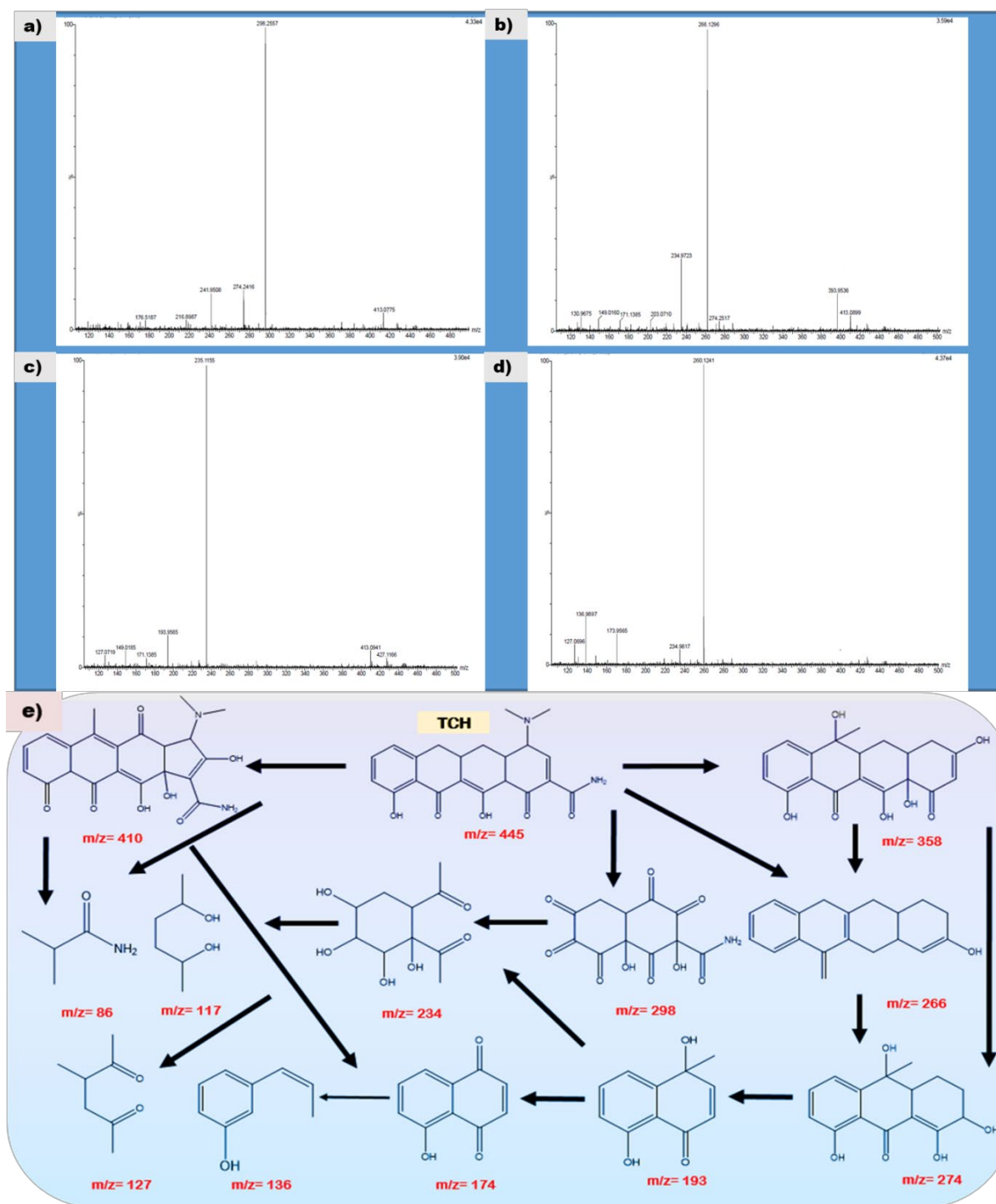| 6	135.9544	134.0732	[M+H]+		
7	116.9843	116.0837	[M]+		
8	98.9742	98.0732	[M]+		

Fig S8. (a-d) LCMS spectra of degradation of TCH at 10, 20, 40, and 60 minutes duration; (e) Plausible degradation pathways for TCH degradation.

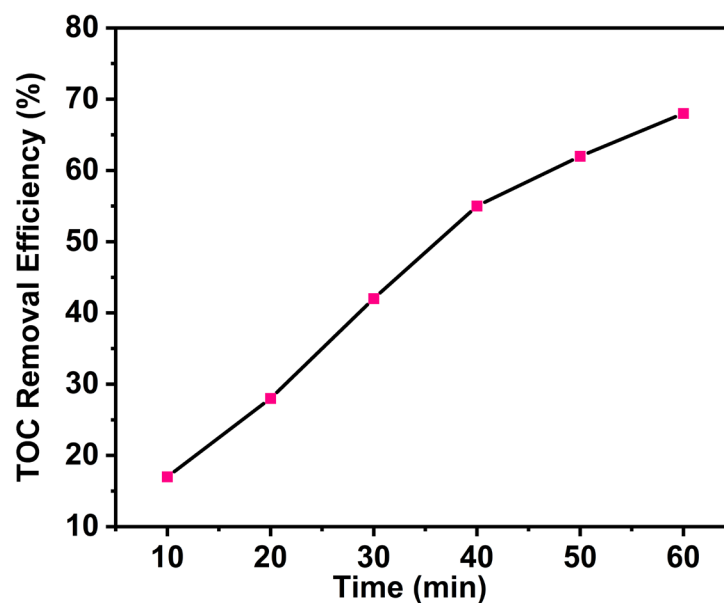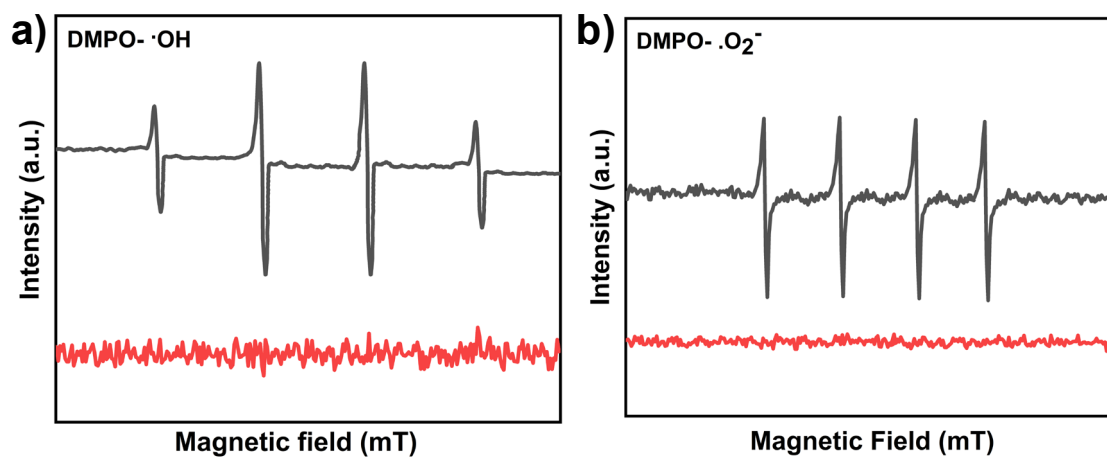**Fig. S9.** Total organic carbon content (in %) after photodegradation.

Fig. S10. ESR spectra representing generation of (a) ·OH radicals, (b) ·O_2^- radicals in light and dark conditions respectively.
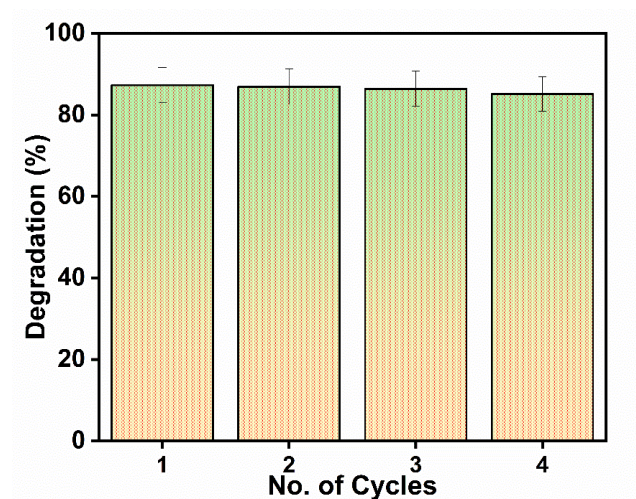
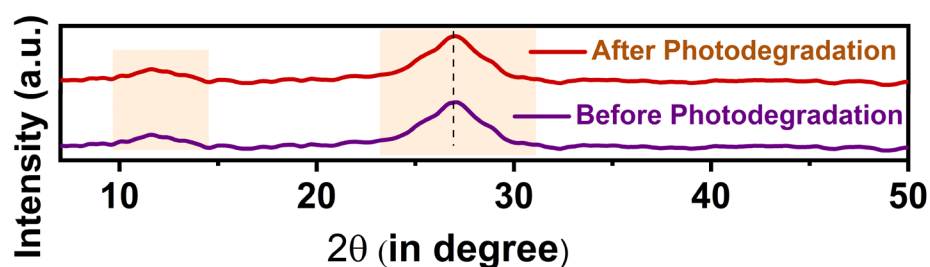**Fig. S11.** Reusability Survey of the fabricated nanocatalyst for degradation of the target pollutant.

Fig. S12. XRD of the fabricated nanocatalyst before and after four consecutive cycles.
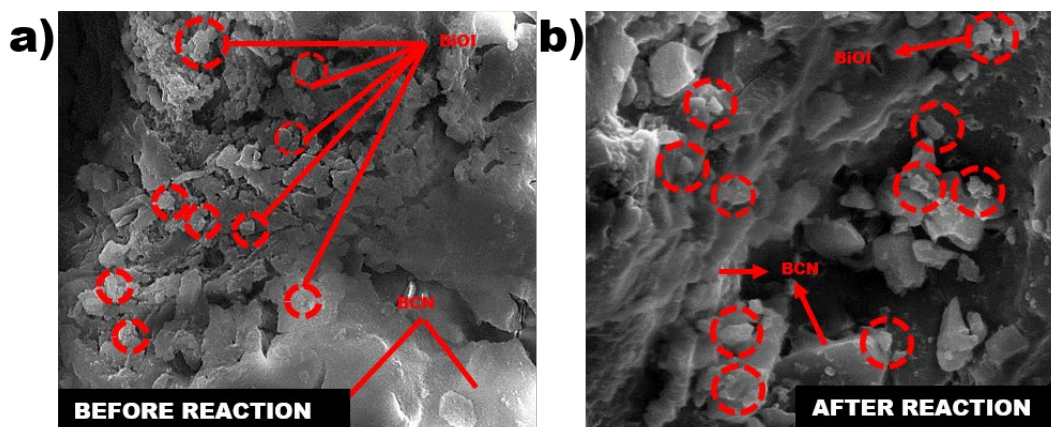

Fig. S13. FESEM of nanocomposite BiOI/BCN-15 before and after photocatalytic degradation.

References

1   Z. Ma, C. Zeng, L. Hu, Q. Zhao, Q. Yang, J. Niu, B. Yao en Y. He, *Appl. Surf. Sci.*, 2019, **484**, 489–500.

2   J. Di, M. Ji, J. Xia, X. Li, W. Fan, Q. Zhang en H. Li, *J. Mol. Catal. A Chem.*, 2016, **424**, 331–341.

3   Y. Wang, Z. Qiang, W. Zhu, W. Yao, S. Tang, Z. Yang, J. Wang, J. Duan, C. Ma en R. Tan, *ACS Appl. Nano Mater.*, 2021, **4**, 8680–8689.

4   M. Mousavi, A. Habibi-Yangjeh en M. Abitorabi, *J. Colloid Interface Sci.*, 2016, **480**, 218–231.

5   S. K. Venkatraman, N. Vijayakumar, D. K. Bal, A. Mishra, B. Gupta, V. Mishra, M. Wysokowski, S. Koppala en S. Swamiappan, *Inorg. Chem. Commun.*, 2022, **142**, 109674.